Engineering Geology 251 (2019) 71–80

Contents lists available at ScienceDirect

Engineering Geology

journal homepage: www.elsevier.com/locate/enggeo

A novel physically-based model for updating landslide susceptibility

H.J. Wang[a], T. Xiao[a], X.Y. Li[b], L.L. Zhang[c], L.M. Zhang[a,*]

[a] Department of Civil and Environmental Engineering, The Hong Kong University of Science and Technology, Clear Water Bay, Kowloon, Hong Kong, China
[b] School of Civil Engineering, Sun Yat-sen University, Guangzhou 510275, China
[c] State Key Laboratory of Ocean Engineering, Shanghai Jiaotong University, 800 Dongchuan Road, Shanghai, China

ARTICLE INFO

Keywords:
Landslide susceptibility
Slope stability
Risk analysis
Bayesian networks
Monte Carlo simulation
Field monitoring

ABSTRACT

A novel physically-based method for updating landslide susceptibility is presented in this paper, considering both spatial and cross correlations. First, a Bayesian network relating landslide susceptibility to spatially and cross correlated soil parameters is constructed for susceptibility assessment. Then, the correlations among the grid cells and the prior probabilities of the Bayesian network are quantified utilizing Monte Carlo simulation and random field theory. After that, observed slope performance information is used to update the landslide susceptibility and the soil parameters. Two case studies were worked out to illustrate the application of the proposed method. It is found that the integration of performance information of certain cells significantly improves the susceptibility evaluation of the adjacent cells and the updated soil properties are closer to the reality. By introducing the Bayesian network to physically-based landslide susceptibility, this method is able to consider the inherent correlations in landslide susceptibility analysis and update regional landslide susceptibility and soil parameters utilizing performance information, effectively improving the accuracy and capacity of physically-based landslide susceptibility analysis.

1. Introduction

Susceptibility assessment plays a significant role in landslide hazard mitigation (Guzzetti et al., 1999; Dai et al., 2002; Van Westen et al., 2008). As given by the Joint Technical Committee on Landslides and Engineered Slopes (JTC-1, 2008; Fell et al., 2008), landslide susceptibility is a quantitative or qualitative assessment of the classification, volume (or area), and spatial distribution of landslides which exist or may potentially occur in an area. Many models have been developed to assess landslide susceptibility, including geomorphological mapping (e.g., Van Westen et al., 2003), heuristic models (e.g., Ruff and Czurda, 2008), statistical and machine learning models (e.g., Remondo et al., 2005; Lin et al., 2009; Huang et al., 2017; Lombardo and Mai, 2018) and physically-based models (e.g., Chen and Zhang, 2014; Chen et al., 2015). Based on these models, numerous case studies have been worked out to conduct regional susceptibility assessments (e.g., Guzzetti et al., 2006; Chang et al., 2011; Shou and Lin, 2016; Basu and Pal, 2018; Mondal and Mandal, 2018). Among these studies, landslide susceptibility zoning is a frequently-used approach to deal with the regional landslide susceptibility problem. By dividing a research area into numerous homogenous cells or domains and ranking these cells according to their degrees of susceptibility, landslide susceptibility zoning is a visualized and convenient way to conduct risk assessment (Van Westen et al., 2008).

Physically-based susceptibility models are widely adopted for landslide zoning. Compared to other models like statistical or heuristic models, a physically-based model features integrating susceptibility analysis with rock and soil mechanics. With information such as geometry of slopes and formation lithology, susceptibility analysis can be conducted based on soil and rock mechanics, giving this method sound physical basis. However, most physically-based susceptibility analyses are a one-off assessment which can hardly respond to the input of monitoring information as inherent correlations of geomaterials are not considered (Li et al., 2015). For example, after a certain event like an earthquake or heavy rainfall (e.g., Fan et al., 2018), many landslides may be observed in a particular region. When such observational information is available, it is difficult to update the susceptibility map using traditional physically-based methods.

Bayesian approach is an effective and widely-used tool to deal with updating problems. For example, slope performance information was used to update input slope parameters and model uncertainties based on Bayes' theorem (Zhang et al., 2010a). Zhang et al. (2010b) also used site-specific slope performance to update single slope reliability through Bayesian back-analysis. Peng et al. (2014) integrated multi-

* Corresponding author.
E-mail addresses: h.wang@connect.ust.hk (H.J. Wang), xiaote@ust.hk (T. Xiao), lixueyou@mail.sysu.edu.cn (X.Y. Li), lulu_zhang@sjtu.edu.cn (L.L. Zhang), cezhangl@ust.hk (L.M. Zhang).

https://doi.org/10.1016/j.enggeo.2019.02.004
Received 31 July 2018; Received in revised form 31 January 2019; Accepted 2 February 2019
Available online 07 February 2019
0013-7952/

source monitoring information to conduct single slope safety evaluation. Li et al. (2016b,c) further combined multi-source time-series monitoring data with three-dimensional numerical analysis to update single slope performance. Among these studies, Bayesian methods for single slope performance updating have been well developed. However, regional slope reliability analysis using monitoring data remains a challenge and the capability of existing updating method is also questionable when facing consecutive monitoring data.

Unlike direct Bayesian updating in previous studies, Bayesian networks are capable of continuous updating. A Bayesian network is the product of graph theory and statistics theory which has strength in solving uncertainty problems by logic reasoning (Jensen and Nielsen, 2007). It is made up of nodes and arcs/links with their (conditional) probabilities and capable of conducting continuous updating with available evidences. The dependencies among the nodes are quantified by their conditional probability tables (CPTs). With the rapid development of this algorithm, several well-developed Bayesian network analysis programs have been released in the last decade (e.g., Hugin Researcher (Hugin Expert A/S, 2009), GeNle (GeNle Academic, 2016)). Even though the Bayesian network emerged in the area of computer science, many applications of Bayesian networks have been made in the engineering field (Peng and Zhang, 2012a,b; Straub and Der Kiureghian, 2010a,b; Li et al., 2017). Nevertheless, few publications have considered the use of Bayesian networks to tackle the bottleneck of susceptibility analysis.

The objective of this paper is to explore the possibility of combining the physically-based susceptibility analysis and Bayesian networks into an enhanced method for susceptibility updating and decision making. In the following parts, a novel probabilistic landslide susceptibility analysis method is presented utilizing observational slope performance information. This method is aimed to (1) consider correlations among geomaterials and (2) update the landslide susceptibility and soil parameters with the input of monitoring data. This paper will first introduce the proposed method for updating landslide susceptibility and soil parameters. Thereafter, two case studies will be presented to illustrate the proposed method.

2. Updating landslide susceptibility using Bayesian networks

2.1. Framework of physically-based landslide susceptibility updating

Landslide susceptibility zoning is realized by discretizing the terrain into finite grid cells. The reliability of each cell is independent of each other in the traditional susceptibility assessment. In the proposed framework, the correlations among grid cells are described in Bayesian networks to link susceptibility of the grid cells. Monitoring information can be used to update the whole Bayesian network. Based on this, the main steps of the proposed methodology are described as follows:

1. Causal Bayesian networks are first constructed based on landslide susceptibility zoning, considering both the spatial and cross correlations of the soil parameters and the relationships among the network nodes.
2. The prior probabilities of the root nodes of the Bayesian network; namely, the prior probabilities of effective cohesion (c') and effective friction angle (ϕ'), are quantified with available site information. Meanwhile, the correlations of the soil parameters is established in this step.
3. The prior susceptibility of leaf nodes, which is the conditional probabilities of the factor of safety (*FS*) nodes given the probability density function (PDF) of the soil parameters, $P(FS|c', \phi')$, is established based on an infinite slope model and Monte Carlo simulation (MCS).
4. The posterior susceptibility is obtained by updating the priors with available records of slope performance. Also, the probability distributions of the soil parameters can be updated using performance information, serving the purpose of making soil parameters more accurate.

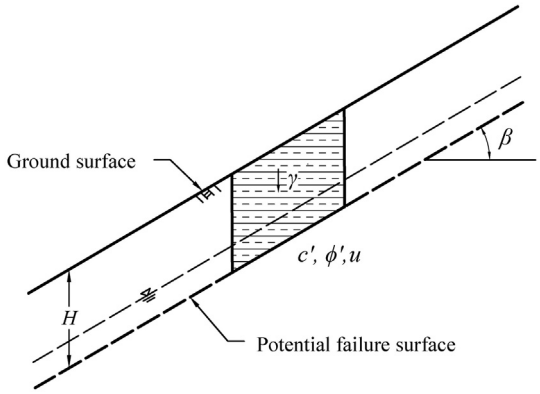

Fig. 1. An infinite slope stability model (modified from Griffiths et al., 2011).

The proposed framework is introduced step by step in the following sections. Then, two examples, one 4-cell susceptibility updating considering both cross and spatial correlations and one 10-cell susceptibility updating considering spatial correlation, are presented to illustrate the proposed method.

2.2. Constructing Bayesian networks considering spatial and cross correlations

Let us first consider a typical slice of infinite slope (e.g., Griffiths et al., 2011) for slope stability evaluation, which is shown in Fig. 1. The factor of safety (*FS*) is given by

$$FS = \frac{(H\gamma\cos^2\beta - u)tan\phi' + c'}{H\gamma\sin\beta\cos\beta} \quad (1)$$

where H is the depth of the soil layer to the potential failure surface; β is the slope inclination; γ is the total unit weight of the soil above the failure surface; u is the pore water pressure at the failure surface; c' and ϕ' are the effective cohesion and effective friction angle of the soil at the failure surface, respectively. Among all the six variables (H, β, γ, u, c' and ϕ') in Eq. (1), the first four (H, β, γ and u) can be regarded as constant parameters since these parameters can be obtained directly from site investigation. The shear strength parameters c' and ϕ' are shown to be highly variable due to geological and transformation uncertainties (Duncan, 2000; Zhou et al., 2018) and taken as random variables, becoming the root nodes of the network. Any changes in the PDFs of the two variables will influence the susceptibility of the grid cells.

Two causal Bayesian networks have been constructed for physically-based landslide susceptibility updating. In Fig. 2(a), only the spatial correlation is considered. Nodes of c' and ϕ' at different locations are connected separately. In Fig. 2(b), both the spatial correlation and the cross correlation between c' and ϕ' are taken into consideration. Hence, links between c' nodes and ϕ' nodes are connected. Correlations among the variables can then be quantified with random field theory, which will be introduced in the next section.

The elements of the two Bayesian networks consist of three basic variable in the Bayesian networks: two root nodes (effective cohesion c' and effective friction angle ϕ') and one leaf node (factor of safety *FS*). These nodes are connected with two arcs/links: c'-*FS* and ϕ' -*FS*. The nodes for c' and ϕ' are taken as continuous nodes while the node for the factor of safety is considered discrete with two states: either ≥ 1 (survival) or smaller than 1 (failure).

Based on the networks constructed, the soil parameter nodes are the parent nodes of the factor of safety. Therefore, if some failure cells are observed after a certain event (e.g., rainfall, earthquake, etc.) and

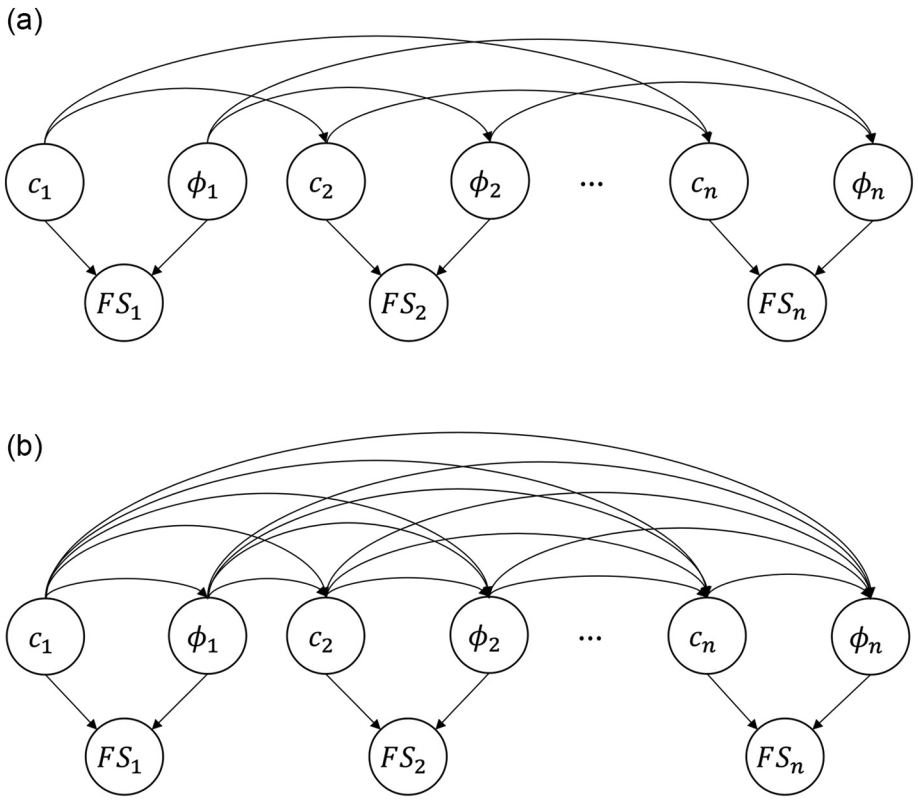

Fig. 2. Bayesian networks for updating landslide susceptibility: (a) considering spatial correlation; (b) considering both spatial and cross correlations.

records of failure are taken as the input of the Bayesian network, changes will immediately take effect on the corresponding parameter nodes. Meanwhile, with the spatial correlation among grid cells, other parameter nodes will also change, ultimately leading to updated susceptibility of all cells. This updating process is strongly physically based: from the aspect of slope failure mechanism, a slip surface tends to develop along weak spots in the ground. As adjacent locations share the similar geological conditions, the stability of any cells near the failure cells may also be considered poor.

2.3. Quantification of prior probabilities using random field theory and Monte Carlo simulation

After the construction of the Bayesian networks, quantifying the prior probabilities of all nodes becomes the next issue. To conduct precise probability updating, discrete variables should not have continuous parents (Jensen and Nielsen, 2007). Therefore, continuous variables need to be discretized. To be specific, we have to specify intervals for a finite set of states for each continuous node in these Bayesian networks. The PDFs of the c' and ϕ' of the soil can be obtained from site investigations. The prior susceptibility of each cell can be calculated using MCS, taking all possible combinations into account:

$$P(FS_i < 1) = \sum_{k=1}^{n_M} P(FS_i < 1, M_k),\ \boldsymbol{i} = 1, 2, \ldots, \boldsymbol{N} \tag{2}$$

where N is the total number of cells; M_k is one possible combination of the material properties (i.e., c' and ϕ') of all cells ($c_{1,p1}$, $c_{2,p2}$, …, $c_{N,pN}$, $\phi_{1,q1}$, $\phi_{2,q2}$, …, $\phi_{N,qN}$); n_M is the total number of possible c' and ϕ' combinations; $c_{N,pN}$ is the effective cohesion of cell N which falls in its $p_N{}^{th}$ interval; $\phi_{N,qN}$ is the effective friction angle of cell N which falls in its $q_N{}^{th}$ interval. To obtain the prior susceptibility described in Eq. (2), random values of c' and ϕ' which fit specified PDFs and correlations are generated using MCS (Bong and Stuedlein, 2018; Zhang et al., 2018) and random field theory (Fenton and Griffiths, 2008; Li et al., 2016a; Tian et al., 2016).

First, to quantify the spatial correlation for the soil parameters, a random field needs to be generated (Juang et al., 2018; Gong et al., 2018). The correlation among the random variables can be quantified using a correlation matrix $\boldsymbol{C}$:

$$\boldsymbol{C} = [\rho(\tau_{ij})] \tag{3}$$

where ρ() is the autocorrelation function; τ_{ij} represents the distance between cells i and j. An exponential autocorrelation function is chosen to characterize the spatial correlation:

$$\rho(\tau_{ij}) = \exp\left(-\frac{2\tau_{ij}}{\theta}\right) \tag{4}$$

where θ is the scale of fluctuation.

Then, to further consider the cross correlation between c' and ϕ' (assuming the correlation coefficient between c' and ϕ' for the same cell is $\rho_{c,\phi}$), a simple model linking spatial and cross correlations is applied in this study (Ji et al., 2012; Xiao et al., 2017):

$$\rho_{c_i,\phi_j} = \rho_{c,\phi} \cdot \rho(\tau_{ij}) \tag{5}$$

where $\rho_{ci,\phi j}$ is the correlation between c_i (effective cohesion of cell i) and ϕ_j (effective friction angle of cell j). Eq. (5) assumes that the spatial variability of c' and ϕ' is identical. Finally, the global correlation matrix $\boldsymbol{Q}$ for c' and ϕ' can be given as:

$$\boldsymbol{Q} = \begin{bmatrix} \boldsymbol{C} & \rho_{c,\phi} \cdot \boldsymbol{C} \\ \rho_{c,\phi} \cdot \boldsymbol{C} & \boldsymbol{C} \end{bmatrix} \tag{6}$$

Now take a random vector, $\boldsymbol{X}$, consisting of uncorrelated random variables which follow the standard normal distribution. The correlated random vector $\boldsymbol{Z}$ considering both spatial and cross correlations can be obtained by

$$\boldsymbol{Z} = \boldsymbol{L}\boldsymbol{X} \tag{7}$$

where $\boldsymbol{L}$ is the Cholesky decomposition matrix satisfying $\boldsymbol{Q} = \boldsymbol{L}\boldsymbol{L}^{\mathrm{T}}$. It is

then converted to c' and ϕ' with other PDFs using the Nataf transformation (Liu and Der Kiureghian, 1986).

After getting the random vector, the corresponding *FS* for each pair of c' and ϕ' can be calculated. For example, assume there are N cells and MCS is conducted N_T times. For cell i, if there are $N_{F,i}$ failure records with $FS_i < 1$ among N_T trials, the prior distribution of susceptibility can be obtained as:

$$P(FS_i < 1) = \frac{N_{F,i}}{N_T} = \frac{\sum_k^{n_M} N_{F,ik}}{N_T} \tag{8}$$

where $N_{F,ik}$ is the number of failure records of cell i under a certain combination of soil properties (M_k) and N_T is the total simulation runs of MCS. Given by Eq. (8), the probability that each *FS* node lies in the failure interval (less than one) is defined as the susceptibility of this cell.

2.4. Updating landslide susceptibility and soil parameters using Bayesian network

Based on Bayes' theorem, the network can be updated when new observations of slope performance are available and the posterior susceptibility can be obtained. For instance, for the susceptibility of cell i given the failure information of a set of cells E_F, the probability is

$$P(FS_i < 1 \mid E_F) = \frac{P(FS_i < 1, E_F)}{P(E_F)} = \frac{\sum_{k=1}^{n_M} P(FS_i < 1, E_F, M_k)}{\sum_{k=1}^{n_M} P(E_F, M_k)} \tag{9}$$

where E_F is the event set of failure cells where $FS < 1$; FS_i is the factor of safety for cell i and n_M is the total number of possible material (i.e., c' and ϕ') combinations.

Besides, if the performance information of some grid cells is known, the probability density functions of the soil parameters can also be updated. For example, for a certain combination of slope performance after a certain hazard event, the probability density distributions of the material properties for all cells can be derived as

$$P(M_k \mid E_F, E_S) = \frac{P(M_k, E_F, E_S)}{P(E_F, E_S)}, \quad k = 1, 2, \ldots, n_M \tag{10}$$

where E_S is the event set of all survival cells where $FS \geq 1$.

3. Illustrative example I: 4-cell susceptibility updating considering both spatial and cross correlations

The landslide susceptibility of a hypothetical study area is evaluated in this example, which is shown in Fig. 3. In this example, an area of $60 \times 60\ m^2$ is selected and discretized into 4 cells $30 \times 30\ m^2$ each cell. With reference to Griffiths et al. (2011), the effective shear strength parameters, c' and ϕ', are assumed to follow the normal distribution with mean values and standard deviations of 10 kPa and 3 kPa for effective cohesion, and 30° and 8.6° for effective friction angle, respectively. Other four parameters are set to be constant values for illustration purposes, which are $\beta = 30°$, $u = 9$ kPa, $H = 5$ m, and $\gamma = 17$ kN/m^3.

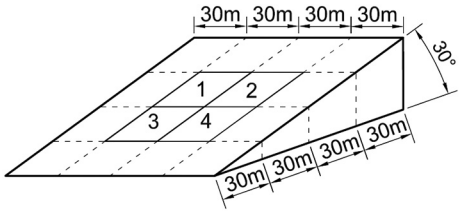

Fig. 3. Sketch of the four-cell landslide susceptibility problem in example I.

3.1. Construction of the causal Bayesian network

Based on the model shown in Fig. 2(b), a Bayesian network which is demonstrated in Fig. 4(a) is constructed in Hugin to integrate observational information and update landslide susceptibility and the PDFs of the soil parameters. As only c' and ϕ' are treated as random variables, the root nodes of this network are the effective cohesion and friction angle of selected four cells $\{c_1 \ldots \ldots c_4\}$ and $\{\phi_1 \ldots \ldots \phi_4\}$, while the leaf nodes of the network are the factor of safety $\{FS_1 \ldots \ldots FS_4\}$. The distributions of c' and ϕ' are discretized into three intervals, while the factor of safety is given two intervals for illustration: either survive (i.e., greater than one) or fail (i.e., less than one). As c' and ϕ' are assumed to follow the normal distribution, the three intervals are extended to six times of standard deviations to ensure accuracy. The specific intervals of the parameters are summarized in Table 1. Note that the cross correlation $\rho_{ci,\phi j}$ between cohesion and friction angle is assumed to be a constant when generating random fields using Eq. (6). As suggested by Wolff (1985), $\rho_{ci,\phi j}$ is set to be -0.47 in the updating process.

3.2. Quantification of the Bayesian network

A major task of quantifying the Bayesian network is to find the prior distributions of all the network nodes. For the c' and ϕ' nodes, their PDFs are known in this case; while for the *FS* nodes, the conditional probability distributions given the PDFs of effective cohesion and friction angle can be obtained through MCS.

To consider the spatial and cross correlations, an autocorrelation matrix of a random field is first generated using Eq. (6). Then, MCS is performed in MATLAB to create randomly correlated c' and ϕ' values which follow the specified normal distributions. In this example, 1×10^6 correlated normal distributed random numbers are generated for every c' or ϕ' node to ensure the simulation of rare cases and the integrity of the conditional probability table.

With the simulation cases generated by MCS, the prior susceptibility of the cells can be evaluated through MCS. By pairing the simulation values of c' and ϕ' for a certain cell, we can calculate the factor of safety for each pair based on Eq. (1). Then, based on the calculated values of factor of safety, simulation cases are classified into different combinations to quantify the prior PDFs of *FS* nodes. In this example, each of the c' and ϕ' nodes has three intervals while the *FS* nodes have two intervals, hence we have 18 combinations for the *FS* nodes. After the classification, the probability that each *FS* node lies in the failure interval (i.e., less than one) is defined as the susceptibility of the cell.

3.3. Updating landslide susceptibility

Even though the prior probability distributions of nodes have been quantified, the data has to be transformed into CPTs before importing to Hugin. With the processed CPTs, the prior susceptibility of all four cells is recalculated within Hugin; the results are summarized in Table 1. For example, the probability that the value of effective cohesion is in State 1 (1 to 7 kPa) is 15.86%, which is consistent with the assumptions. Due to the simulation error given by MCS, the probability values of a certain state of different cells differ slightly. When the performance information of cells is available, the susceptibility can be updated.

For illustration purposes, four scenarios, which are listed in Table 2, are analyzed in this example, corresponding to different combinations of failure modes (one cell fails; two cells fail; three cells fail). The process of Hugin updating is shown in Fig. 4(b). Each piece of observational information will cause changes in the probability distributions for all other nodes in the network. For example, as shown in Fig. 4(b), the FS nodes of cells 1 is set to "Fail" in scenario 1, causing the updating of PDFs of all other nodes. The results of those four scenarios are listed in Fig. 5. From Fig. 5, it can be found that there is a negative correlation between the increment of susceptibility and the separation distance: the increment of the susceptibility of the target cell decreases

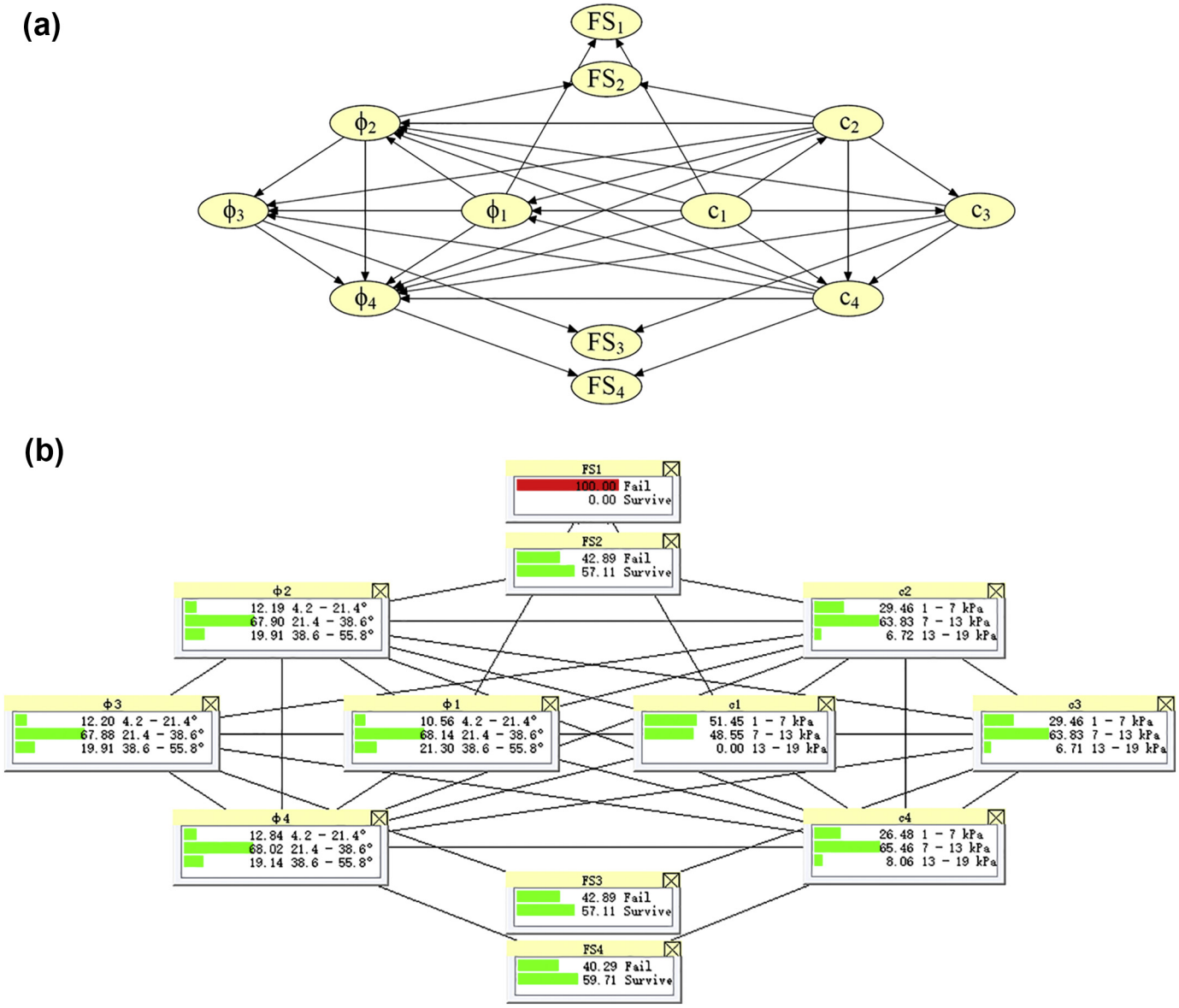

Fig. 4. (a) Bayesian network for example I (4 cells) that considers both spatial and cross correlations; (b) Updating the Bayesian network using Hugin (Scenario I: Cell 1 fails).

Table 1
Nodes, states and the prior probability of the Bayesian networks for examples I and II.

Nodes	Example I		Example II	
	States	Prior (%)	States	Prior (%)
Effective cohesion (kPa)	1 to 7	15.86 ± 0.03	2 to 4	15.86 ± 0.06
	7 to 13	68.27 ± 0.03	4 to 6	68.27 ± 0.08
	13 to 19	15.86 ± 0.03	6 to 8	15.86 ± 0.06
Effective friction angle (°)	4.2 to 21.4	15.86 ± 0.03	23.1 to 29.7	15.86 ± 0.07
	21.4 to 38.6	68.27 ± 0.03	29.7 to 36.3	68.27 ± 0.04
	38.6 to 55.8	15.86 ± 0.03	36.3 to 42.9	15.86 ± 0.06
Factor of safety	Fail ($FS < 1$)	34.97 ± 0.03	Fail ($FS < 1$)	2.81 to 42.65
	Survive ($FS \geq 1$)	65.03 ± 0.03	Survive ($FS \geq 1$)	57.35 to 97.19

as the distance of the failure cell from the target cell increases. Also, the more the surrounding cells fail, the higher the susceptibility of the target cell will be. Besides, the integration of observed slope performance information can significantly enhance the susceptibility assessment. For instance, when three cells fail, the maximum susceptibility reaches 60%, which is more than twice the prior susceptibility.

3.4. Updating probability distributions of soil parameters

Apart from updating the landslide susceptibility, we can also use the Bayesian network to update the PDFs of the soil parameters. For illustration purpose, only updating results of cell 4 are shown in this section. Fig. 6 shows the updated cumulative distribution functions (CDFs) of c' and ϕ' for cell 4 under different scenarios. There is an obvious negative correlation between the effective cohesion and friction angle. As shown in Fig. 7, as more cells fail from scenarios I to IV, the mean value of effective cohesion keeps decreasing while that of effective friction angle keeps increasing. It can also be found that the susceptibility is more sensitive to the effective cohesion in this example.

Table 2
Scenarios for 4-cell landslide susceptibility updating (example I).

Type of scenarios	Scenarios	Input information for landslide susceptibility updating	Input information for soil parameter updating
One cell fails	I	Cell 1 fails	Cell 1 fails; other cells survive
Two cells fail	II	Cells 1, 2 fail	Cells 1, 2 fail; other cells survive
	III	Cells 2, 3 fail	Cells 2, 3 fail; other cells survive
Three cells fail	IV	Cells 1, 2, 3 fail	Cells 1, 2, 3 fail; other cells survive

3.5. Parametric study on the scale of fluctuation

Based on Eq. (4), the scale of fluctuation is an essential factor which affects the correlation among the cells. So, a parametric study targeting the effect of scale of fluctuation is performed in this section. For illustration purposes, only results of scenario I are presented in this section. The scale of fluctuation is considered the same in the horizontal and vertical directions, and θ values of 10, 30, 60, 180, 360 and 1800 m are tested through the Bayesian network.

As shown in Fig. 8, when $\theta = 10$ m, which is much smaller than the cell spacing (30 m), the failure cells barely influence the surrounding cells. The updated results are almost identical with the prior. However, in the situation where the scale of fluctuation is 1800 m, the cells are closely correlated, and the maximum updated susceptibility reaches 56.31% with only one surrounding cell fail.

The results indicate that when the scale of fluctuation is small, the correlation between the cells is weak. In this case, the increment of the susceptibility of the cells that arises from the failure of adjacent cells is negligible. In contrast, when the scale of fluctuation is large, the correlation is very strong, which leads to a significant increment of updated susceptibility.

3.6. Parametric study on the c'–ϕ' cross correlation

To study the influence of parameter cross correlation, different values of the $c'-\phi'$ correlation coefficient are examined. Based on

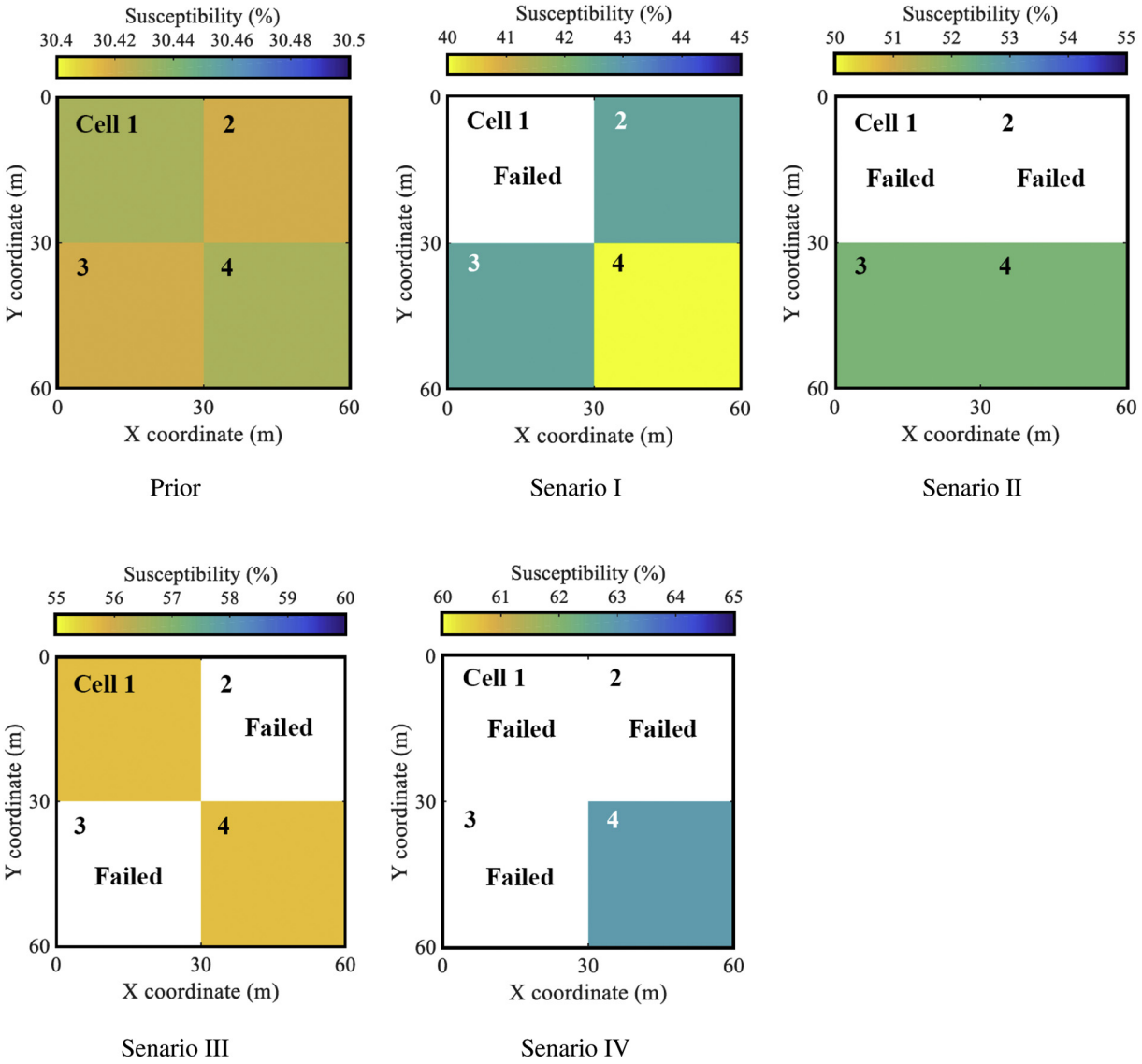

Fig. 5. Results of 4-cell landslide susceptibility updating.

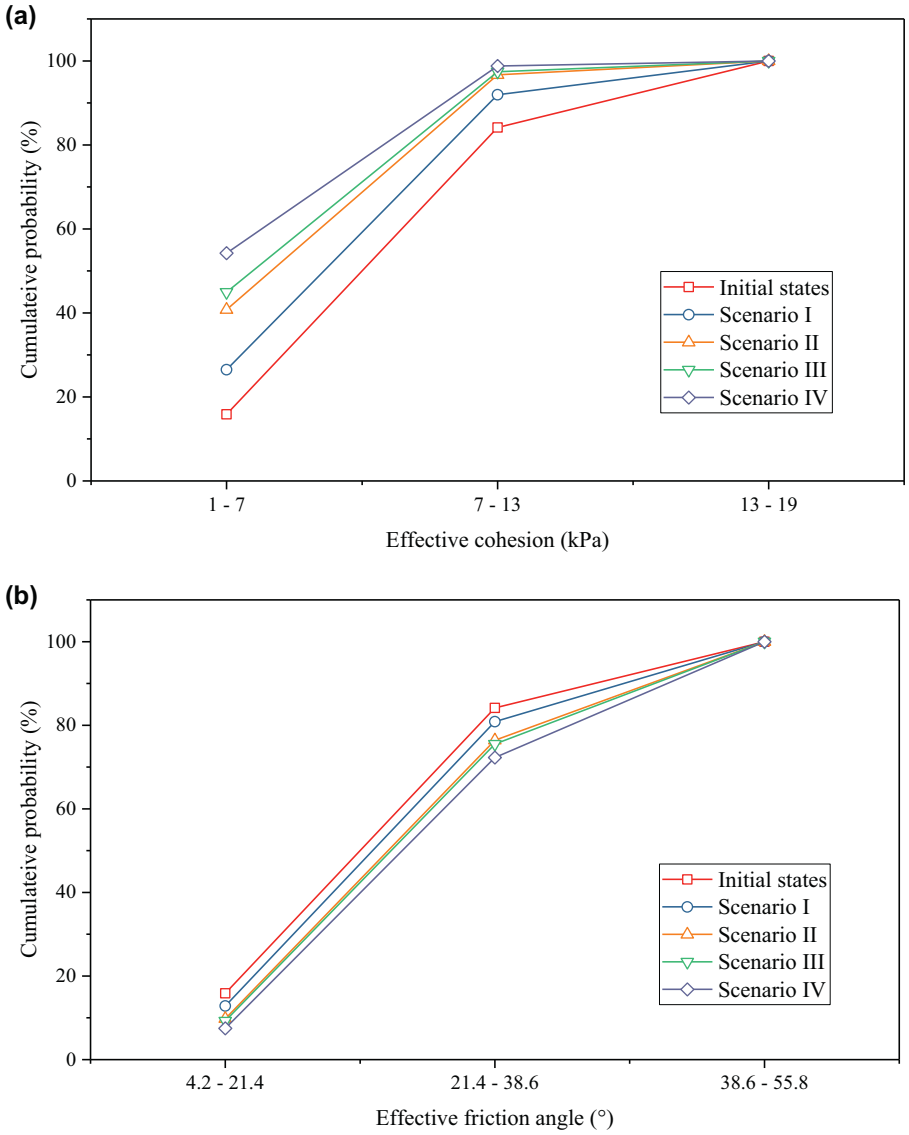

Fig. 6. Results of updated distributions of soil parameters for cell 4: (a) updated probability distributions of effective cohesion; (b) updated probability distributions of effective friction angle.

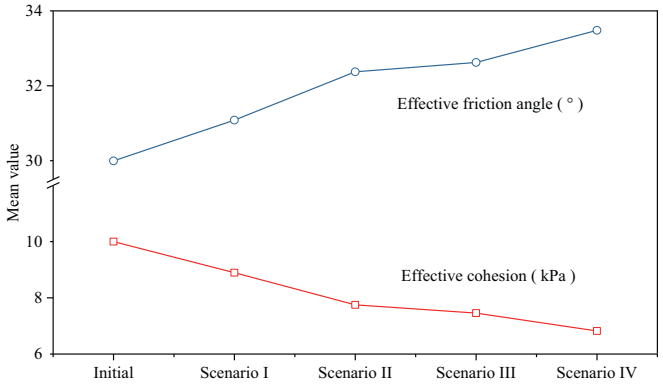

Fig. 7. Mean values of effective cohesion and friction angle under different scenarios.

previous studies (Yucemen, 1973; Lumb, 1970), several values of the cross correlation coefficient, $\rho_{c,\phi} = 0, -0.3, -0.4, -0.5, -0.6, -0.7$, are studied in this section and results are summarized in Fig. 9. As symmetrical cells share the similar susceptibility, only typical values are shown in this figure. Based on the figure, given the same initial parameters, it can be found that the prior susceptibility increases along with the correlation coefficient $\rho_{c,\phi}$. However, as $\rho_{c,\phi}$ increases, interestingly, the increment of susceptibility decreases. Besides, it can be found that the stronger the negative cross correlation is, the higher the increment of susceptibility will be. Apparently, the model which considers the $c'-\phi'$ correlation is closer to the reality. Overall, different values of correlation coefficient do not lead to significant changes in the susceptibility. Neglecting the $c'-\phi'$ correlation will slightly overestimate the susceptibility but underestimate the increment of susceptibility.

4. Illustrative example II: 10-cell updating considering spatial correlation

For further illustration, an existing slope located at the western Lantau Island, Hong Kong is studied. As neglecting the $c'-\phi'$ correlation does not affect the results significantly, this example only considers the spatial correlation. As shown in Fig. 10, a cluster of open hillslope failures occurred on a hillside above Tai O San Tsuen during the June

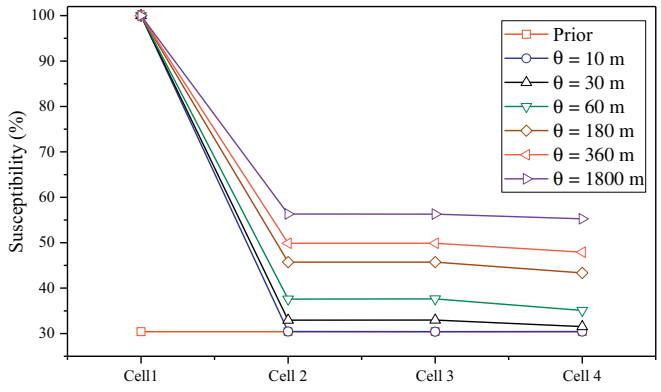

Fig. 8. Results of a parametric study on scale of fluctuation.

2008 rainstorm. According to the Enhanced Natural Terrain Landslide Inventory (ENTLI) records and the field investigation report by GEO (2011), six landslides were identified in this area in 2008 but the field investigation only covered five of them. Hence, in this example, an area of 40 × 100 m^2 is selected and discretized into 10 cells 20 × 20 m^2 each. Four landslides are within the selected area; the three investigated landslides are taken as observations and the one not investigated is taken as validation case.

Since the material of the landslide mass is mainly colluvium, according to Zhu et al. (2018), the soil unit weight (γ = 19 kN/m^3) is taken as a constant and the mean values of c' and ϕ' are set to 5 kPa and 33°, respectively. Based on Cho (2010), the coefficient of variation is taken as 0.2 for c' and 0.1 for ϕ'. The slope inclination is calculated for each cell based on a 0.5 m resolution digital elevation model of Lantau Island. The slope angles of cells 1–10 are 33.61°, 36.43°, 31.36°, 24.59°, 35.34°, 32.69°, 35.96°, 26.08°, 31.32°, 37.13°, respectively. The soil depth (H) is set as 2 m with reference to the site investigation results. The ground water table is assumed to be at 0.5 m above the failure surface and the pore water pressure u is calculated for each cell accordingly.

4.1. Updating landslide susceptibility of the study area

Based on the model shown in Fig. 2(a), a Bayesian network is constructed to integrate the observational information (Fig. 11). The major difference between the two Bayesian networks in Figs. 4(a) and 11 is that the c'–ϕ' correlation is considered in Fig. 4(a) through the arcs/links between the c' and ϕ' nodes. The specific intervals of the c' and ϕ' nodes are also summarized in Table 1. The quantification process is similar to that of the previous example.

After the quantification, with the processed CPTs of nodes c', ϕ' and FS, the prior susceptibility of all the ten cells is calculated in Hugin, and the susceptibility is then updated by setting cells 2, 5 and 10 to fail. Both the prior and updated results are presented in Fig. 12. Before the updating, it can be found that 80% of the area is stable with susceptibility < 30%. After integrating the failure information of cells 2, 5 and 10, the susceptibility of the whole area increases, especially for cell 7 whose susceptibility has changed from 28.34% to 62.55%. The drastic increase in the susceptibility of cell 7 reveals that this cell is highly susceptible to landslide under the condition that cells 2, 5 and 10 fail. Apart from cell 7, other cells remain stable, with the highest susceptibility of 27.09% for cell 1. The record from ENTLI database proves that a landslide indeed happened at the location of cell 7 in 2008, which verifies the accuracy of the updated susceptibility results.

4.2. Computational challenges

Hugin is used in the illustrative examples due to its strength in graphic display of networks and operational convenience. However, restrictions have been encountered in the analysis. Assume N cells need to be evaluated and updated, and each of the parameter nodes is given r states. When considering only the spatial correlation, the size of the largest conditional probability table (CPT) for a single node will reach r^N. When considering both the spatial and c'–ϕ' correlations, the size of the largest CPT will increase significantly to r^{2N}. For example, in the 10-cell updating, if considering both correlations, the largest CPT size for a single node will reach 3^{20}. In the 32-bit version of Hugin employed in this paper, a warning message 'Node table too large' for memory outflow will pop up when processing such large CPTs. To tackle this problem, reducing the size of CPTs or links of the Bayesian network is an effective solution. How to update landslide susceptibility for hundreds or thousands of cells is a challenging topic for future study.

5. Conclusions

A physically-based landslide susceptibility model considering the correlations of grid cells is proposed, and its feasibility for susceptibility and soil parameter updating is confirmed. Other than updating the susceptibility of a single slope, continuous updating of regional

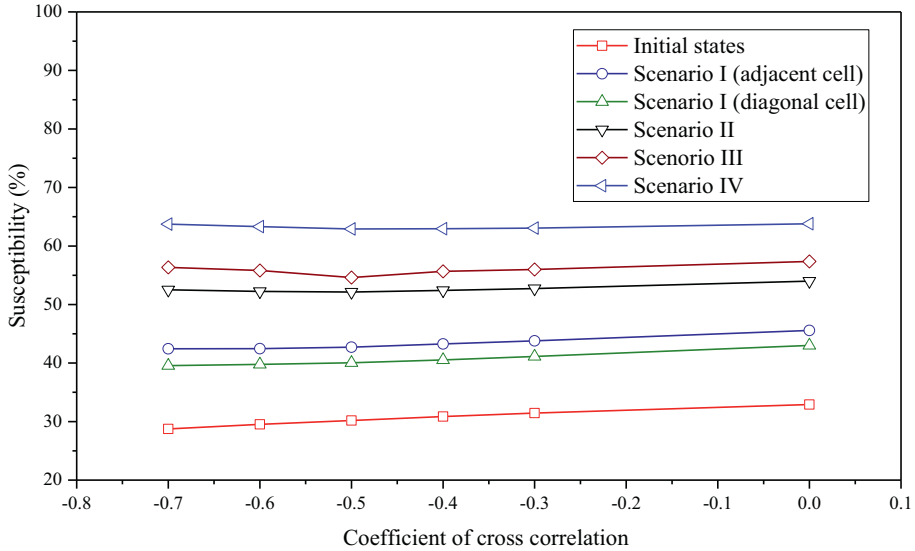

Fig. 9. Results of a parametric study on c'–ϕ' correlation.

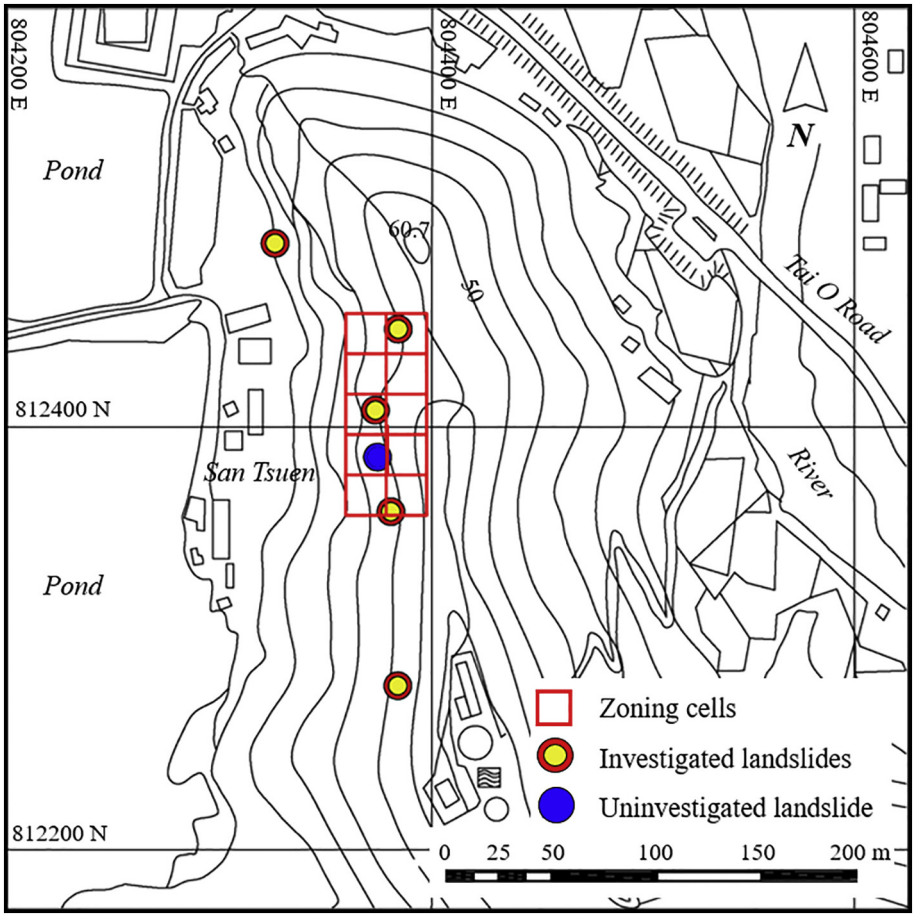

Fig. 10. Site and zoning condition in example II.

landslide susceptibility is made possible through the proposed method utilizing Bayesian networks. Observational information on slope performance can be integrated into the Bayesian networks continuously so that the landslide susceptibility of all the cells can be updated.

Bayesian networks are first constructed considering both the spatial and cross correlations between effective cohesion and friction angle. Monte Carlo simulation and random field theory are then used to quantify the prior distributions of the Bayesian networks. Based on the

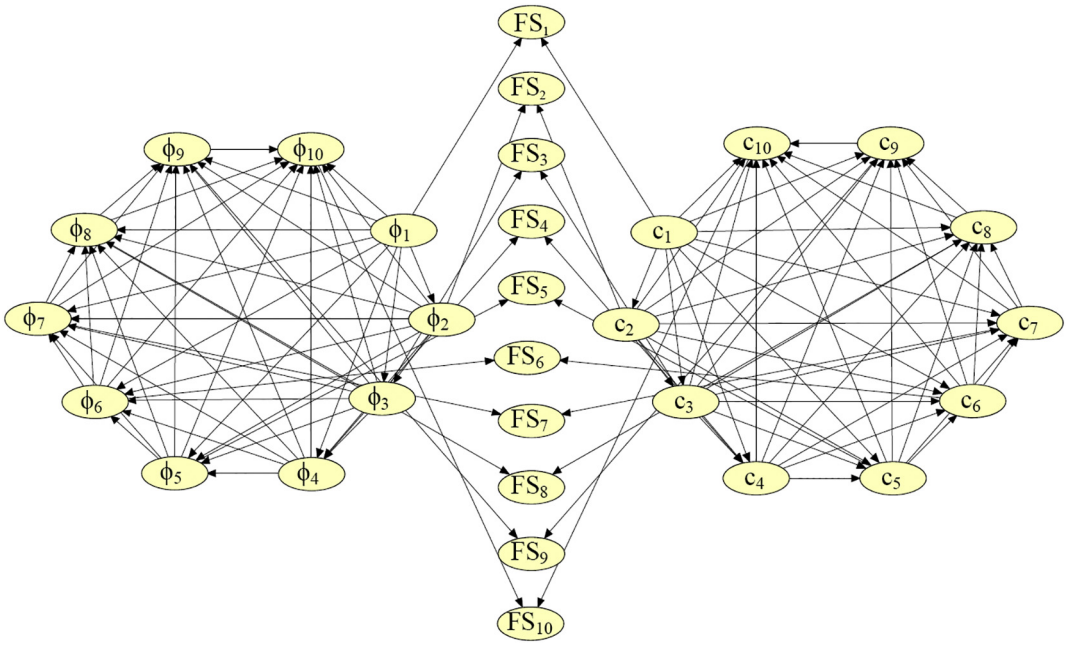

Fig. 11. Bayesian network for example II (10 cells) considering spatial correlation.

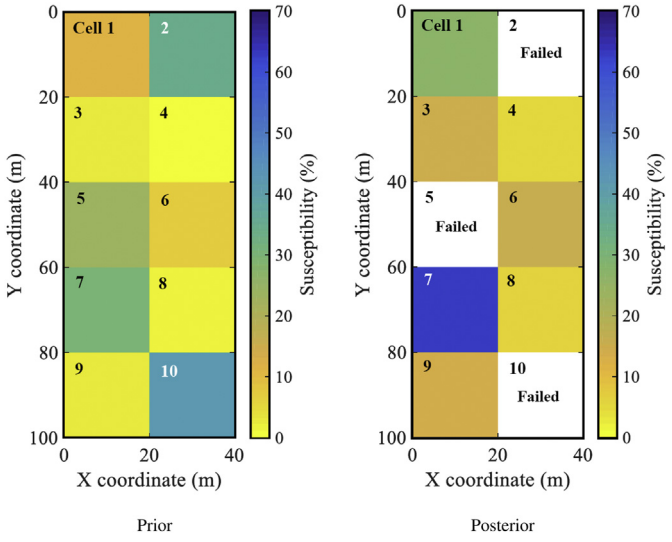

Fig. 12. Results of the susceptibility updating in example II.

constructed Bayesian networks, observed slope performance information can be set as input for the networks, thereby to update the landslide susceptibility of the entire area. In this process, both the susceptibility of the slope cells and the probability distributions of the soil parameters can be updated through this exercise.

During the updating, the scale of fluctuation measures the intensity of spatial correlation: a higher scale of fluctuation will build stronger spatial correlation, making cells more sensitive to failure of adjacent cells, and vice versa. The model considering the *c'–φ'* cross correlation is closer to the real world. Neglecting the cross correlation will slightly overestimate the initial susceptibility but underestimate the increment of susceptibility.

Acknowledgments

This research is supported by the Research Grants Council of the Hong Kong SAR Government (Nos. 16202716 and C6012-15G).

References

Basu, T., Pal, S., 2018. Identification of landslide susceptibility zones in Gish River basin, West Bengal, India. Georisk: Assess. Manage. Risk Eng. Syst. Geohazards 12 (1), 14–28.
Bong, T., Stuedlein, A.W., 2018. Efficient methodology for probabilistic analysis of consolidation considering spatial variability. Eng. Geol. 237, 53–63.
Chang, S.K., Lee, D.H., Wu, J.H., Juang, C.H., 2011. Rainfall-based criteria for assessing slump rate of mountainous highway slopes: a case study of slopes along Highway 18 in Alishan, Taiwan. Eng. Geol. 118 (3–4), 63–74.
Chen, H.X., Zhang, L.M., 2014. A physically-based distributed cell model for predicting regional rainfall-induced shallow slope failures. Eng. Geol. 176, 79–92.
Chen, H.X., Zhang, L.M., Gao, L., Zhu, H., Zhang, S., 2015. Presenting regional shallow landslide movement on three-dimensional digital terrain. Eng. Geol. 195, 122–134.
Cho, S.E., 2010. Probabilistic assessment of slope stability that considers the spatial variability of soil properties. J. Geotech. Geoenviron. 136 (7), 975–984.
Dai, F.C., Lee, C.F., Ngai, Y.Y., 2002. Landslide risk assessment and management: An overview. Eng. Geol. 64 (1), 65–87.
Duncan, J.M., 2000. Factors of safety and reliability in geotechnical engineering. J. Geotech. Geoenviron. 126 (4), 307–316.
Fan, X., Juang, C.H., Wasowski, J., Huang, R., Xu, Q., Scaringi, G., van Westen, C.J., Havenith, H.B., 2018. What we have learned from the 2008 Wenchuan Earthquake and its aftermath: a decade of research and challenges. Eng. Geol. 241, 25–32.
Fell, R., Corominas, J., Bonnard, C., Cascini, L., Leroi, E., Savage, W.Z., 2008. Guidelines for landslide susceptibility, hazard and risk zoning for land-use planning. Eng. Geol. 102 (3), 99–111.
Fenton, G.A., Griffiths, D.V., 2008. Risk Assessment in Geotechnical Engineering. John Wiley & Sons, Hoboken, NJ.
GeNIe Academic, 2016. BayesFusion, LLC. https://www.bayesfusion.com/ Accessed 20 Aug 2018.
GEO, 2011. GEO Report No. 275. Geotechnical Engineering Office, Hong Kong SAR.
Gong, W., Juang, C.H., Ii, J.R.M., Tang, H., Wang, Q., Huang, H., 2018. Probabilistic analysis of tunnel longitudinal performance based upon conditional random field simulation of soil properties. Tunn. Undergr. Space Technol. 73, 1–14.
Griffiths, D.V., Huang, J., Fenton, G.A., 2011. Probabilistic infinite slope analysis. Comput. Geotech. 38 (4), 577–584.
Guzzetti, F., Carrara, A., Cardinali, M., Reichenbach, P., 1999. Landslide hazard evaluation: a review of current techniques and their application in a multi-scale study, Central Italy. Geomorphology 31 (1), 181–216.
Guzzetti, F., Reichenbach, P., Ardizzone, F., Cardinali, M., Galli, M., 2006. Estimating the quality of landslide susceptibility models. Geomorphology 81 (1–2), 166–184.
Huang, F., Yin, K., Huang, J., Gui, L., Wang, P., 2017. Landslide susceptibility mapping based on self-organizing-map network and extreme learning machine. Eng. Geol. 223, 11–22.
Hugin Expert A/S, 2009. Hugin Researcher. http://www.hugin.com/index.php/hugin-developerhugin-researcher/, Accessed date: 20 August 2018.
Jensen, F.V., Nielsen, T.D., 2007. Bayesian Networks and Decision Graphs. Springer, New York.
Ji, J., Liao, H.J., Low, B.K., 2012. Modeling 2-D spatial variation in slope reliability analysis using interpolated autocorrelations. Comput. Geotech. 40, 135–146.
JTC-1, 2008. Joint ISSMGE, ISRM and IAEG Technical Committee on Landslides and Engineered Slopes. https://www.isrm.net/gca/?id=307, Accessed date: 20 August 2017.
Juang, C.H., Gong, W., Martin, J.R., Chen, Q., 2018. Model selection in geological and geotechnical engineering in the face of uncertainty - does a complex model always outperform a simple model? Eng. Geol. 242, 184–196.
Li, D.Q., Jiang, S.H., Cao, Z.J., Zhou, W., Zhou, C.B., Zhang, L.M., 2015. A multiple response-surface method for slope reliability analysis considering spatial variability of soil properties. Eng. Geol. 187, 60–72.
Li, D.Q., Xiao, T., Cao, Z.J., Zhou, C.B., Zhang, L.M., 2016a. Enhancement of random finite element method in reliability analysis and risk assessment of soil slopes using Subset simulation. Landslides 13 (2), 293–303.
Li, X.Y., Zhang, L.M., Jiang, S.H., Li, D.Q., Zhou, C.B., 2016b. Assessment of slope stability in the monitoring parameter space. J. Geotech. Geoenviron. 142 (7), 04016029.
Li, X.Y., Zhang, L.M., Jiang, S.H., 2016c. Updating performance of high rock slopes by combining incremental time-series monitoring data and three-dimensional numerical analysis. Int. J. Rock Mech. Min. Sci. 83, 252–261.
Li, X.Y., Zhang, L.M., Zhang, S., 2017. Efficient Bayesian networks for slope safety evaluation with large quantity monitoring information. Geosci. Front. 9 (6), 1679–1687. https://doi.org/10.1016/j.gsf.2017.09.009.
Lin, H.M., Chang, S.K., Wu, J.H., Juang, C.H., 2009. Neural network-based model for assessing failure potential of highway slopes in the Alishan, Taiwan area: Pre-and post-earthquake investigation. Eng. Geol. 104 (3–4), 280–289.
Liu, P.L., Der Kiureghian, A., 1986. Multivariate distribution models with prescribed marginals and covariances. Prob. Eng. Mech. 1 (2), 105–112.
Lombardo, L., Mai, P.M., 2018. Presenting logistic regression-based landslide susceptibility results. Eng. Geol. 244, 14–24.
Lumb, P., 1970. Safety factors and the probability distribution of soil strength. Can. Geotech. J. 7 (3), 225–242.
Mondal, S., Mandal, S., 2018. RS & GIS-based landslide susceptibility mapping of the Balason River basin, Darjeeling Himalaya, using logistic regression (LR) model. Georisk: Assess. Manag. Risk Eng. Syst. Geohazards 12 (1), 29–44.
Peng, M., Zhang, L.M., 2012a. Analysis of human risks due to dam-break floods—part 1: a new model based on Bayesian networks. Nat. Hazards 64 (1), 903–933.
Peng, M., Zhang, L.M., 2012b. Analysis of human risks due to dam break floods—part 2: application to Tangjiashan landslide dam failure. Nat. Hazards 64 (2), 1899–1923.
Peng, M., Li, X.Y., Li, D.Q., Jiang, S.H., Zhang, L.M., 2014. Slope safety evaluation by integrating multi-source monitoring information. Struct. Saf. 49, 65–74.
Remondo, J., Bonachea, J., Cendrero, A., 2005. A statistical approach to landslide risk modelling at basin scale: from landslide susceptibility to quantitative risk assessment. Landslides 2 (4), 321–328.
Ruff, M., Czurda, K., 2008. Landslide susceptibility analysis with a heuristic approach in the Eastern Alps (Vorarlberg, Austria). Geomorphology 94 (3–4), 314–324.
Shou, K.J., Lin, J.F., 2016. Multi-scale landslide susceptibility analysis along a mountain highway in Central Taiwan. Eng. Geol. 212, 120–135.
Straub, D., Der Kiureghian, A., 2010a. Bayesian network enhanced with structural reliability methods: methodology. J. Eng. Mech. 136 (10), 1248–1258.
Straub, D., Der Kiureghian, A., 2010b. Bayesian network enhanced with structural reliability methods: Application. J. Eng. Mech. 136 (10), 1259–1270.
Tian, M., Li, D.Q., Cao, Z.J., Phoon, K.K., Wang, Y., 2016. Bayesian identification of random field model using indirect test data. Eng. Geol. 210, 197–211.
Van Westen, C.J., Rengers, N., Soeters, R., 2003. Use of geomorphological information in indirect landslide susceptibility assessment. Nat. Hazards 30 (3), 399–419.
Van Westen, C.J., Castellanos, E., Kuriakose, S.L., 2008. Spatial data for landslide susceptibility, hazard, and vulnerability assessment: an overview. Eng. Geol. 102 (3–4), 112–131.
Wolff, T.H., 1985. Analysis and Design of Embankment Dam Slopes: A Probabilistic Approach. Ph.D. thesis. Purdue University, Lafayette, Ind.
Xiao, T., Li, D.Q., Cao, Z.J., Tang, X.S., 2017. Full probabilistic design of slopes in spatially variable soils using simplified reliability analysis method. Georisk: Assess. Manag. Risk Eng. Syst. Geohazards 11 (1), 146–159.
Yucemen, M.S., 1973. A Probabilistic Study of Safety and Design of Earth Slopes. Ph.D. thesis. University of Illinois at Urbana-Champaign, Urbana, Ill.
Zhang, L.L., Zhang, J., Zhang, L.M., Tang, W.H., 2010a. Back analysis of slope failure with Markov chain Monte Carlo simulation. Comput. Geotech. 37 (7), 905–912.
Zhang, J., Zhang, L.M., Tang, W.H., 2010b. Slope reliability analysis considering site-specific performance information. J. Geotech. Geoenviron. 137 (3), 227–238.
Zhang, L.L., Wu, F., Zheng, Y., Chen, L., Zhang, J., Li, X., 2018. Probabilistic calibration of a coupled hydro-mechanical slope stability model with integration of multiple observations. Georisk: Assess. Manage. Risk Eng. Syst. Geohazards 12 (3), 169–182.
Zhou, X.P., Zhu, B.Z., Juang, C.H., Wong, L.N.Y., 2018. A stability analysis of a layered-soil slope based on random field. Bull. Eng. Geol. Environ. 1–15.
Zhu, H., Zhang, L.M., Xiao, T., 2018. Evaluating the stability of anisotropically deposited soil slopes. Can. Geotech. J. https://doi.org/10.1139/cgj-2018-0210.